DOI: 10.1017/S1431927603443924
Microsc Microanal 9(Suppl 2), 2003

Measurement of Charge at Grain-boundary Edge Dislocations in Ca-doped and Undoped YBCO by Electron Holography

M. A. Schofield[*], M. Beleggia[*], Y. Zhu[*], K. Guth[**], Ch. Jooss[**]

[*]Department of Materials Science, Brookhaven National Laboratory, Upton, Long Island NY 11973
[**]University of Göttingen, Windausweg 2, 37073 Göttingen, Germany

Grain boundaries present the major factor limiting high current applications in high-temperature superconductors.[1] Various mechanisms have been proposed to understand grain boundary (GB) transport properties, and the recently discovered increase of the intergranular J_c by hole doping in $YBa_2Cu_3O_{7-x}$ (YBCO) through Ca substitution of Y suggests that electronic band bending and charge depletion may be responsible for the suppression of superconductivity.[2] To address this issue, we made a comparison study of 20% Ca-doped and Ca-free, 4° [001] tilt boundaries in YBCO thin films grown by laser ablation on $SrTiO_3$.[3] Compared to large-angle GBs, small-angle GBs offer the possibility for space-charge measurement of separated interfacial dislocation cores when they are probed edge-on.

Figure 1(a) shows a high-resolution image of the Ca-doped YBCO where undisturbed crystal lattices between the ~5.3 nm periodically disordered interfacial dislocation cores are clearly visible. Electron holography experiments were carried out under identical imaging conditions in a 300 kV JEOL 3000F FEG for both doped and undoped YBCO bicrystals. Holograms were recorded with 50V biprism bias, 37x37nm^2 field of view, 650kX magnification and 2.8Å interference fringes. To improve phase sensitivity, at least 5 holograms from the same region of each sample were recorded. The phase contribution from the bulk crystal was subtracted from the total phase[4] to give phase maps, $\phi_{GB}(\mathbf{r})$, representing only the GB dislocations, and are shown in Fig.1(b-d). The projected GB potential, $V_{GB}(\mathbf{r})$, is then related to the phase by $\phi_{GB}(\mathbf{r}) = C_E t V_{GB}(\mathbf{r})$, where C_E=6.25x10^{-3} rad/V nm for 300kV electrons and t is the thickness of the sample. Thickness was measured from energy filtered images of both doped and undoped samples, and was found to be 40 and 25 nm for the Ca-free and Ca-doped samples respectively. Due to the approximately radial symmetry about each dislocation core, we extract the measured potential as a function of distance only from the core center, and combine profiles from a number of dislocation cores from each sample as shown in Fig.2. These measurements give clear and direct evidence that Ca-doping in YBCO acts to diminish both the potential drop (from V_{GB}=2.4±0.3V to V_{GB}=1.0±0.1V) and the spatial extent (from D=1.7±0.3nm to D=0.8±0.2nm) of the core potential associated with these GB dislocations.

To further understand the current limiting aspects of the dislocation cores, the charge distribution was calculated from the measured potential by Poisson's equation (both, in real space and Fourier space) in accordance with the Thomas-Fermi screening theory. Specifically, the total charge density, ρ_{tot}, was modeled as the result of two contributions: ρ_{core} due to charge intrinsic to the dislocation, and ρ_{ind} due to an induced rearrangement of mobile charge. Within this model, two parameters, ρ_0 and R, describe the core charge, while a third parameter, the Thomas-Fermi screening length, r_0, describes the response of the induced charge. We considered several core charge models, which were fit in both real-space and Fourier-space, and the results of a Gaussian core charge distribution, $\rho_{core}(r) = \rho_0 e^{-r^2/R^2}$, are summarized in Table I.[3] The total potential arising from this model is shown as continuous lines in Fig.2, and the resulting charge densities are shown in Fig.3. We find that the factor 2 decrease in the potential for the Ca-doped vs. undoped samples is due to a net doping of an average 0.5 electron holes per unit cell at the dislocation. Further, we find a corresponding decrease in the depletion radius of charge carriers, which is the underlying mechanism for improved GB properties by Ca-doping. This direct evidence of charge depletion at the dislocation cores explains the suppression of the critical current, as the hole depletion is directly related to the suppression of the superconducting condensate.[5]

References
1. Hilgenkamp, H., and Mannhart, J., *Rev. Mod. Phys*. **74**, 485-549 (2002).
2. Hammerl, G., *et al.*, *Nature* **407**, 162-164 (2000).
3. Schofield, M. A., *et al.*, submitted to Nature, January 2003.
4. Schofield, M. A., Wu, L. and Zhu, Y., *Phys. Rev. B*, accepted (2002).
5. This work was supported under US DOE contract No. DE-AC02-98CH10886.

TABLE I: Measured values of 4° [001] tilt boundary in Ca-doped and undoped YBCO thin films.

	Potential, V_{GB}	Depletion Radius, D	Max. Charge Density, ρ_0	Core Radius, R	Screening Length, r_0	Total Core Charge, Q_{tot}
YBCO	**2.4±0.3V**	**1.7±0.3nm**	**-0.47 e/unit cell**	**0.98Å**	**2.4Å**	**-9.5e/c-axis**
Ca-YBCO	**1.0±0.1V**	**0.8±0.2nm**	**-0.77 e/unit cell**	**0.47Å**	**1.3Å**	**-3.5e/c-axis**

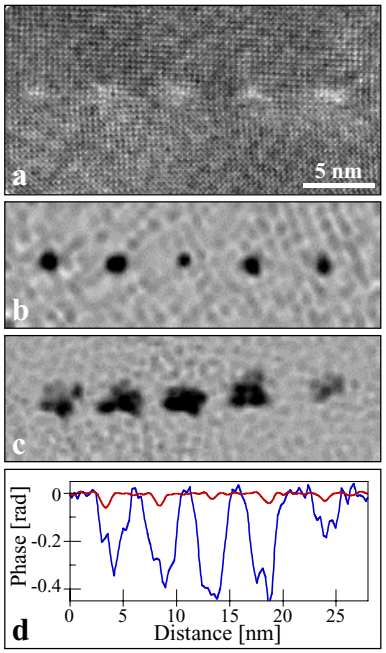

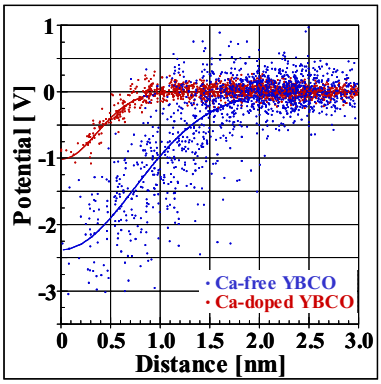

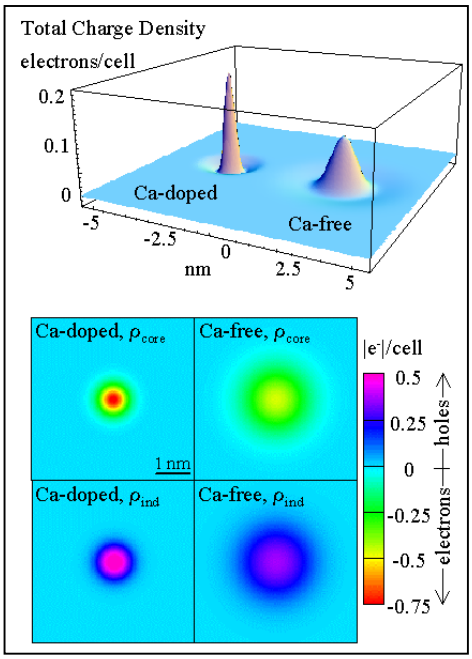

FIG 1. (left) High-resolution image (a) of 4° [001] tilt boundary in Ca-doped YBCO thin film viewed along the [001] direction. Reconstructed phase image showing portions of the 4° [001] tilt boundary in the Ca-doped (b) and undoped (c) YBCO and corresponding phase line profiles (d; red: doped, blue: undoped).

FIG 2. (center) Measured electrostatic potential as a function of distance from the center of dislocation cores in Ca-doped (red) and undoped (blue) YBCO. Each data set (doped and undoped) represents potential values extracted from 5 cores. The solid lines are the fitting results following the model of a Gaussian core charge distribution.

FIG 3. (right) Total charge distribution (top) around dislocation cores for Ca-doped (left) and undoped (right) YBCO. The core and induced charge density (bottom) are shown as color density maps for the dislocation cores in the doped (left) and undoped (right) samples.

https://doi.org/10.1017/S1431927603443924 Published online by Cambridge University Press